PHILOSOPHICAL MAGAZINE B, 1999, VOL. 79, NO. 2, 223–237

The kinetics of the photo-induced solid-state chemical reaction in Ag/$As_{33}S_{67}$ bilayers and its reaction products

T. WAGNER†, E. MÁRQUEZ‡, J. FERNÁNDEZ-PENA§,
J. M. GONZÁLEZ-LEAL‡, P. J. S. EWEN¶ and S. O. KASAP‖

† Department of General and Inorganic Chemistry, University of Pardubice, 53210 Pardubice, Czech Republic
‡ Departamento de Fisica de la Materia Condensada, Universidad de Cadiz, Apdo. 40, 11.510 Puerto Real, Cadiz, Spain
§ Departamento de Ingenieria Electrica, Universidad de Cadiz, Apdo. 40, 11.510 Puerto Real, Cadiz, Spain
¶ Department of Electrical Engineering, University of Edinburgh, Edinburgh EH9 3JL Scotland, UK
‖ Department of Electrical Engineering, University of Saskatchewan, Saskatoon S7N 5A9, Canada

[*Received 7 January 1998 and accepted 30 May 1998*]

ABSTRACT

The kinetics of the photo-induced solid-state chemical reaction of silver with amorphous $As_{33}S_{67}$ films in a conventional sandwich structure was measured by monitoring the change in thickness of the undoped chalcogenide using a modified computer-controlled reflection technique. The reaction between silver and the chalcogenide layer was induced by an Ar-ion laser. The Ag/$As_{33}S_{67}$ sample was illuminated by the laser beam coming from the chalcogenide side of the sample. The consumption of the elemental silver source in the course of the reaction was monitored by the simultaneous measurement of the electrical resistance of the silver layer. The kinetic data obtained show that there are two stages in the photoreaction process, with the second stage having a sublinear dependence. The exhaustion of the elemental silver source in the course of the reaction does not significantly influence the reaction rate. The reaction rates characterizing each stage have been measured, and a comparison of the composition and structure has been made. All the structure-sensitive parameters, T_g, C_p and ΔC_p, measured by the temperature modulated differential scanning calorimetry (MDSC) technique, show a change in the structure of $As_{33}S_{67}$ as silver is introduced by photodoping or in melt-quenched Ag–As–S glasses. Further, by using far-infrared spectroscopy it was possible to correlate the MDSC results to the structure of $As_{33}S_{67}$ and Ag–As–S glasses.

§1. INTRODUCTION

Metal photodissolution (PD) in amorphous chalcogenides was first reported by Kostyshin *et al.* (1966), thirty years ago. This phenomenon has been comprehensively reviewed by Kolobov and Elliott (1991). Interest in this effect, known also as photodiffusion or photodoping, has been partly stimulated by a desire to fully understand the mechanism of the photo-stimulated solid-state reaction and partly by its numerous potential applications in optical recording and more recently, diffractive optics or optical integrated circuits for infrared (IR) operation, which requires thick structures (e.g. 5 μm) to be made in the chalcogenide films. The knowledge of the reaction kinetics during the photoinduced Ag reaction with the chalcogenide layer is

0141–8637/99 $12·00

of prime interest for understanding the mechanism of the reaction, and for meaningful design and also for preparing the optical structures using the PD process.

The PD reaction kinetics and reaction product has been studied recently using many techniques (e.g. measurement of the optical transmittance (Fernandez-Pena *et al.* 1996), X-ray diffraction (Wagner *et al.* 1987)). We choose for our kinetic study the most convenient and reliable reflectivity technique, first developed by Firth *et al.* (1985), and modified by Ewen *et al.* (1988), and Wagner *et al.* (1993, 1996) and Marquez *et al.* (1995). The silver layer thickness during the course of the reaction was determined according to the technique first proposed by Goldschmidt and Rudman (1976) and later improved by Marquez *et al.* (1991), which is based on the measurement of the variation of the electrical resistance of the silver film. The dependence of the electrical resistivity of a silver film on its thickness has been determined by a novel method (Fernandez-Pena *et al.* 1996), based on the *simultaneous* measurements of the optical transmittance and the electrical resistance. The bilayer system $Ag/As_{33}S_{67}$ was chosen because a *homogeneous* reaction product was expected to arise from the PD reaction process for this particular combination.

§2. Experimental procedures

The films of Ag (thickness ≈ 200 nm) and $As_{33}S_{67}$ (thickness ≈ 1400 nm) used in the present work were prepared by thermal evaporation (in about 1×10^{-4} Pa vacuum) in a conventional thermal evaporation unit (Edwards, model E306A), onto cleaned glass substrates. The Ag and $As_{33}S_{67}$ films were evaporated from pure Ag (99.9 at.% Ag) and fragments of the melt-quenched $As_{33}S_{67}$ glass. Electron microprobe analysis of $As_{33}S_{67}$ films indicated that the stated composition is correct to $\pm 0{\cdot}5$ at.%. Ag was evaporated from an Al_2O_3-covered wolfram basket, thereby reducing the heat and light exposure of samples.

The optical reflectivity technique used to measure the photodissolution rate is that developed by Firth *et al.* (1985). Our experimental set-up is shown in detail in figure 1 and is a significant improvement on the technique used by Firth *et al.* (1985), and in particular it employs a computer to read all input and output signals (illumination, reflected light intensity and electrical resistance). The illumination of the samples was carried out by an Ar-ion laser (Omnichrome model 543-AP, $\lambda = 514{\cdot}5$ nm, light intensity ≈ 200 mW cm^{-2}). The angle of incidence was nearly 10°. The laser beam was chopped and a lock-in amplifier (EG&G, model 5104) was used to detect the reflected light. All optical measurements were made at room temperature.

The change in electrical resistance of the silver layer was used to monitor the source of elemental silver during the photodissolution process. As has been previously mentioned, a change in the electrical resistance of the dissolving Ag layer can be related to its thickness (Fernandez-Pena *et al.* 1996). The necessary calibration curve of the electrical resistivity of the silver layer versus silver thickness can be seen in figure 2, and the corresponding expression can be found in Fernandez-Pena *et al.* (1996). Very significantly, the precise moment, t_e, when the Ag layer is *completely* exhausted can *not* be seen as a sharp change in the photodissolution kinetics obtained by the optical reflectivity technique. A micro-ohmmeter (Keithley 580), using a square-wave signal, was employed to measure the electrical resistance of the Ag strips, to avoid the Joule self-heating or electromigration effects, caused by a constant electrical potential applied to the silver layer.

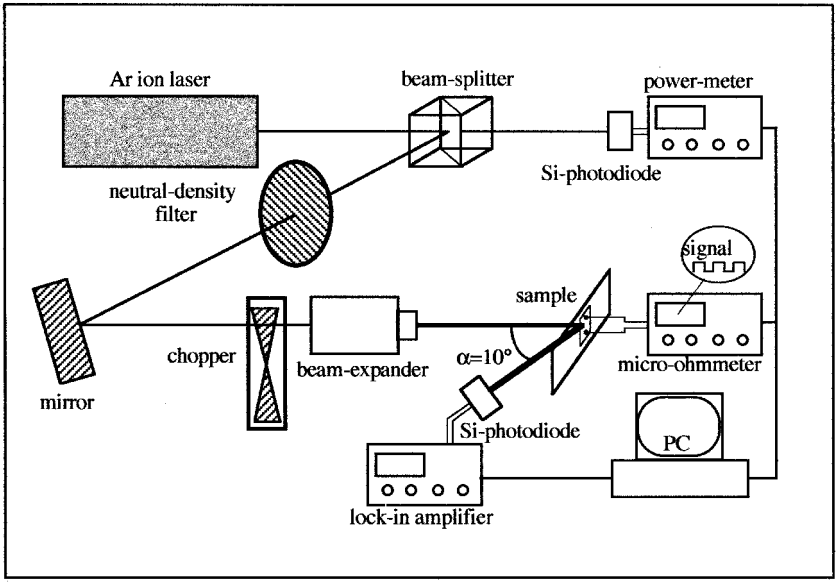

Figure 1. Experimental set-up for the simultaneous measurement of the electrical resistance and the optical reflectivity during the photodissolution process.

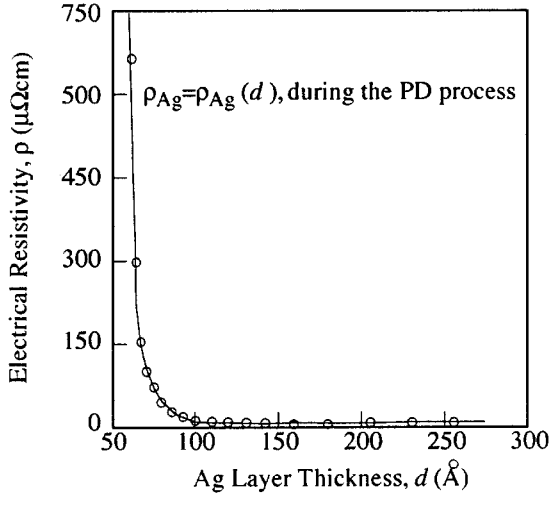

Figure 2. Calibration curve of the electrical resistivity versus thickness of the silver layer.

The procedure used to measure accurately the rate of PD is based on the periodic variation of the reflectivity of a *weakly absorbing* layer with its thickness, due to the interference between the light reflected from the top and bottom surfaces of the layer. A typical plot of reflectivity as a function of exposure time during one of these experiments is shown in figure 3. The time between successive maxima or minima in the curve corresponds to the time required for the thickness of the undoped layer to decrease by $\lambda/2n$, or the doped layer to increase by $c\lambda/2n$, where λ is the wavelength of the detected light (as has been previously mentioned, $\lambda = 514.5$ nm), n is

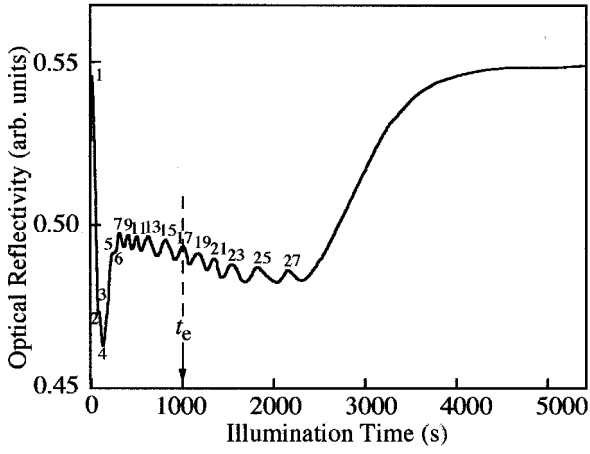

Figure 3. A typical plot of optical reflectivity as a function of illumination time for the $Ag/As_{33}S_{67}$ bilayer system.

the refractive index of the undoped $As_{33}S_{67}$ layer at this particular wavelength ($n = 2{\cdot}57$) and c is a constant relating the thickness of the doped layer to the thickness of the undoped material consumed during the PD effect. At the end of the photodissolution process the thickness of the undoped layer is *zero*, so that the maxima and minima occur when the $As_{33}S_{67}$ layer thickness is an integer multiple of $\lambda/4n$, this integer being 1 for the last minimum, 2 for the last maximum, and so on. In other words, there is an interference condition for the optical reflectivity in this particular case, $4nd = m\lambda$, where d is the layer thickness and m is an integer, so-called the order number, being odd for minima and even for maxima. The correctness of the optical reflectivity technique is clearly supported by the large difference in the Tauc gap ($\Delta E_{g\,opt} \approx 0{\cdot}55$ eV) and refractive index, $n(\Delta n \approx 0{\cdot}5)$, which was found between doped and undoped $As_{33}S_{67}$ glass films (Kosa *et al.* 1995).

Photodoped and undoped samples were thermally analysed by using a novel technique called modulated differential scanning calorimetry (MDSC). MDSC, as a new experimental method, has been described in more detail in the original papers (Reading 1993, Reading *et al.* 1993, Reading *et al.* 1994, Wunderlich *et al.* 1994, Sauerbrunn and Thomas 1995). MDSC operates essentially in the same way as a typical heat flux differential scanning calorimetry (DSC) (Reading 1993), but with an option that allows the sample temperature to be modulated sinusoidally around a constant ramp, i.e. the temperature T at time t is:

$$T = T_0 + rt + A\sin\left(\frac{2\pi t}{P}\right), \tag{1}$$

where T_0 is the initial (or starting) temperature, r is the heating rate, A is the amplitude of the modulation and P is the period. The resulting instantaneous heating rate dT/dt therefore varies sinusoidally around the average heating rate r. The apparatus measures both the amplitude of the instantaneous heat flow and the average heat flow, called the total heat flow, and then by carrying out a suitable Fourier deconvolution of the measured quantities (also incorporating the sinusoidal temperature signal), it determines two quantities: reversing heat flow (RHF) and non-reversing heat flow (NHF).

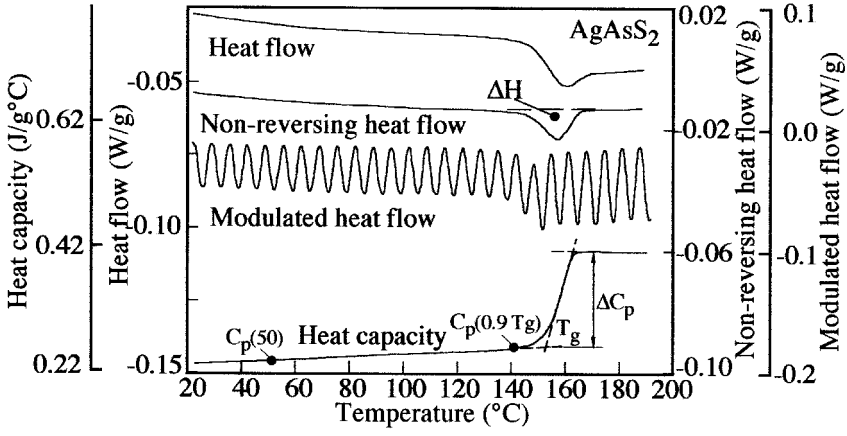

Figure 4. Typical conventional DSC (HF) and MDSC (MHF, NHF and heat capacity) results, during a heating scan in $AgAsS_2$ glass.

For the MDSC measurements the bulk samples ($As_{33}S_{67}$, $AgAsS_2$, Ag_3AsS_3) were crushed into small pieces, and the evaporated films ($As_{33}S_{67}$) and photodoped films (Ag–$As_{33}S_{67}$) were both mechanically peeled from the substrates, and immediately weighed in aluminum crimped pans and then properly sealed. A typical bulk and film sample weight was approximately 18 mg.

The MDSC experiments were carried out as described previously (Wagner and Kasap 1996). Initially, the same thermal history was set up for all samples, in the non-modulated regime. Thus, the modulated regime was applied to measure the modulated heat flow, in heating schedule, in the temperature region 20–240°C. For the present experiments $r = 5°C\,min^{-1}$, $A = \pm 1{\cdot}061°C$ and $P = 80$ s, in equation (1). The specific heat capacity C_p was calculated from the RHF. The C_p measurement by MDSC typically have reproducibilities better than $\pm 1\%$ T_g and ΔC_p were determined from the step transition of the heat capacity in the glass transition region and is shown together with heat flow, non-reversing and modulated heat flow, in figure 4. The mean random error in T_g was $\pm 0{\cdot}1°C$.

The structures of the reaction products and undoped $As_{33}S_{67}$ layers were established from their corresponding far-IR spectra, measured in a Fourier transform infrared (FTIR) spectrometer (Bio-Rad). IR spectra were measured on polyethylene (far-IR quality) tablets, containing the studied materials.

§3. Results

3.1. *Kinetics of optically induced Ag-dissolution in $As_{33}S_{67}$ glass films*

The kinetics of silver dissolution was monitored by making use simultaneously of two independent techniques. The monitoring of the electrical resistance of the silver layer is certainly a very important tool to establish accurately the time t_e when all the elemental silver source is completely consumed during the PD process, as shown in figure 3. The electrical resistance change during the PD phenomenon can be seen in figure 5 (it is worth mentioning that in the present case the value of t_e is approximately 1000 s), where the corresponding plot of the silver layer thickness versus exposure time is also shown. We have calculated the initial silver-consumption rate ν_{Ag}($\nu_{Ag} = 1.27\,nm\,s^{-1}$), as is shown in the inset of figure 5.

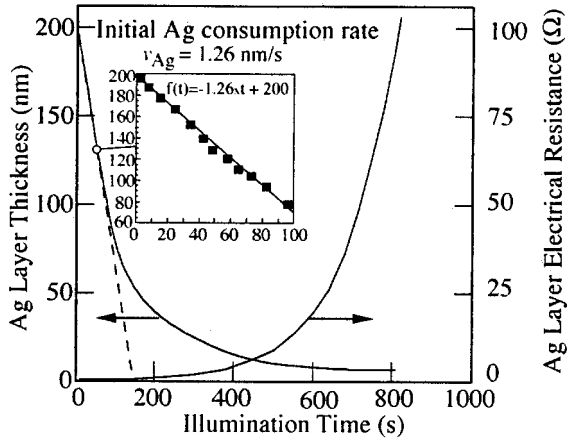

Figure 5. The Ag-layer thickness and Ag electrical resistance versus illumination time during the PD process.

The reflectivity oscillation curve (i.e. the position of the maxima and minima) in figure 3 was used to derive the experimental points for the kinetic curves in figure 6. As can be seen from the reflectivity curve, the oscillation amplitude decreases gradually with time and at a certain point dies out, and then the value of the reflectivity increases monotonically to a new level. The intensity change in the reflectivity curve during the PD process can be attributed to the changing refractive index of the reflecting layer, from that of the initial, elemental Ag layer to that of an $As_{33}S_{67}$ layer, doped with different levels of Ag. The final increase of the reflectivity at the end of the PD effect is certainly due to the leading edge of the boundary (doped/undoped) region, reaching the top surface of the film, so that the Ag-concentration at this surface then gradually increases up to a constant value (18 at.% Ag–see below). From a comparison of the electrical resistance and the optical reflectivity kinetic curves in figures 5 and 6, it is clear that the photodissolution process continues, very significantly, even after the Ag layer is used up and Ag exhaustion has *no* effect on the PD kinetic curve.

In order to find the best physical model to describe and interpret our experimental data corresponding to the metal-dissolution kinetic measurements, we have used in the present study three different fitting functions, as displayed in figure 6. These kinetic fitting curves are the following: (i) simple square root model: $f_1(t) = A_1 t^{1/2}$, where A_1 is a rate coefficient; (ii) two-stage exponential/linear model: $f_2(t) = A_2 \exp(-B_2 t) + C_2 t + D_2$, where B_2 and C_2 are the rate coefficients, and A_2 and D_2 are two constants; (iii) two-stage exponential/square root model: $f_3(t) = A_3 \exp(-B_3 t) + C_3 t^{1/2} + D_3$, where B_3 and C_3 are the rate coefficients, A_3 and D_3 are two constants.

It was found that the *measured* kinetic curve (i.e. doped layer thickness versus exposure time), shown in figure 6, has a more complex character than was usually reported, and cannot be fitted by a simple square root function (for example Kolobov *et al.* (1991)), as shown in figure 6(*a*). A much more realistic approach is to fit the experimental data using *composite* functions, as shown in figure 6(*b*) and (*c*), consisting either of a single exponential and a steady state term, described previously by Wagner *et al.* (1993) or of a single exponential and a square root term.

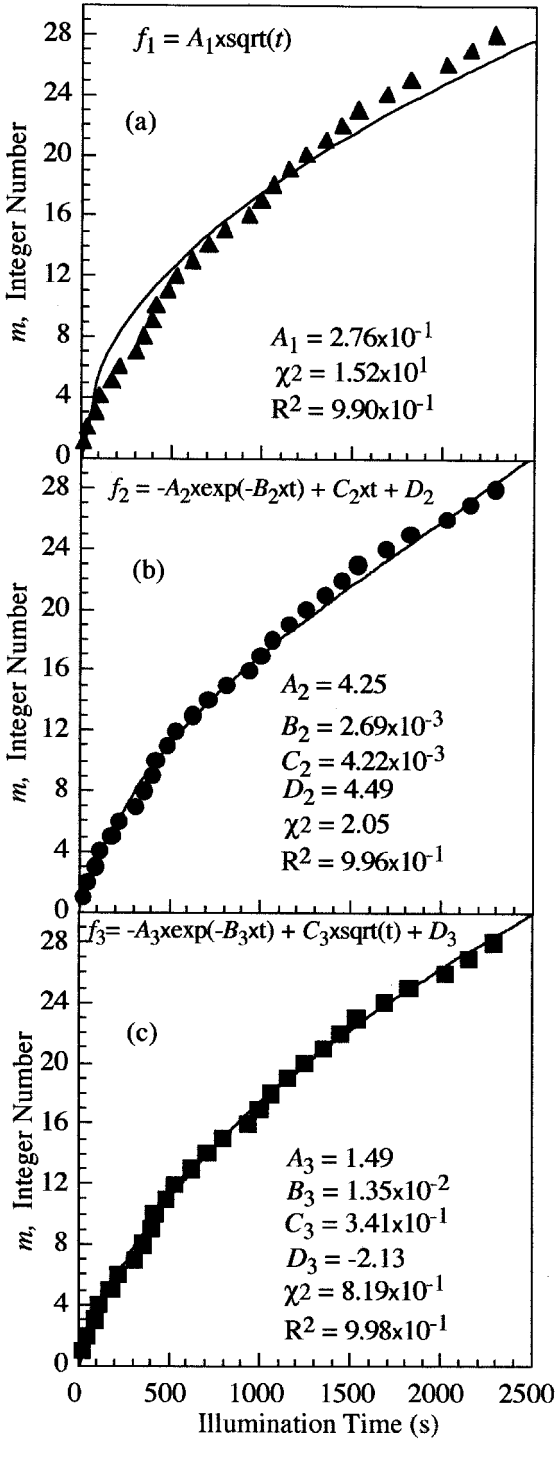

Figure 6. A typical kinetic curve for photodoping of Ag into a As$_{33}$S$_{67}$ glass film. The integer number, m, plotted vertically, is proportional to the photodoped layer thickness. (Solid lines are fits to the experimental points.) The parameters A_1, B_1, C_1, D_2 and χ^2 etc. are all defined in the text.

The values of all the associated fitted parameters are given in the corresponding plot in figure 6. The values for the square of the regression coefficient R^2 and chi-squared χ^2 appear at the bottom of each plot in figure 6. χ^2 is defined as follows:

$$\chi^2 = \sum_i \{[y_i - f(x_i)]/\sigma_i\}^2, \tag{2}$$

where y_i is the y component of the data, x_i is the x component of the data, $f(x_i)$ is the value of the right-hand side of the model equation, evaluated by substituting x_i for the independent variable, σ_i is the weight associated with each data point, and the sum, $\sum_i$, is taken over all the categories in the data selection. It is very clear, indeed, from the results of calculating R^2 and χ^2, given in figure 6, that the best fit is provided by a composite function consisting of a single exponential and a square root term.

The first composite function (a single exponential and a steady state term) and a typical fit to the experimental data are shown in figure 6(*b*). The values of the fitting parameters are: $A_2 = 4{\cdot}26$, $B_2 = 2{\cdot}7 \times 10^{-3}$, $C_2 = 4{\cdot}2 \times 10^{-3}$ and $D_2 = 4{\cdot}49$. The rate coefficients B_2 and C_2 ($B_2 = k_{1,\mathrm{exp}}$ and $C_2 = k_{1,\mathrm{lin}}$, with units s^{-1}) can be converted to the reaction rates, $\nu_{1,\mathrm{exp}}$, and $\nu_{1,\mathrm{lin}}$, by multlplying by $\lambda/2n$, yielding typical values, such as: $\nu_{1,\mathrm{exp}} = 0{\cdot}27\,\mathrm{nm\,s}^{-1}$ and $\nu_{1,\mathrm{lin}} = 0{\cdot}42\,\mathrm{nm\,s}^{-1}$. The parameter A_2 corresponds to the doped layer thickness at the end of stage 1 and start of stage 2. The constant D_2 defines the offset of the steady-state term. The kinetic curve shows that there are two different stages in the PD phenomenon: the first stage is characterized by the rate coefficient $k_{1,\mathrm{exp}}$ and the second stage by $k_{1,\mathrm{lin}}$ where it is verified: $k_{1,\mathrm{exp}} < k_{1,\mathrm{lin}}$.

The second composite function (a single exponential and a square root term) and a typical fit to the experimental data are shown in figure 6(*c*) and the values of the fitting parameters are the following: $A_3 = 1{\cdot}49$, $B_3 = 1{\cdot}35 \times 10^{-2}$, $C_3 = 3{\cdot}41 \times 10^{-1}$ and $D_3 = -2{\cdot}13$. The parameters B_3 and C_3 are again rate coefficients ($B_3 = k_{2,\mathrm{exp}}$ with unit s^{-1}, and $C_3 = k_{2\,\mathrm{sqrt}}$, with unit $\mathrm{s}^{-1/2}$) and can be converted to the reaction rates $\nu_{2,\mathrm{exp}}$ and $\nu_{2,\mathrm{sqrt}}$ by multiplying by $\lambda/2n$ with typical values, such as: $\nu_{2,\mathrm{exp}} = 1{\cdot}27\,\mathrm{nm\,s}^{-1}$ and $\nu_{2,\mathrm{sqrt}} = 34{\cdot}13\,\mathrm{nm\,s}^{1/2}$ (the value of $(\nu_{2,\mathrm{sqrt}})^2$ can be related to the diffusion coefficient with units $\mathrm{nm}^2\,\mathrm{s}^{-1}$, as explained in the discussion section). The parameter A_3 corresponds to the doped layer thickness at the end of stage 1. The constant D_3 defines the offset of the square root term. In this case, the first stage of the two-stage PD process is characterized by the rate coefficient $k_{2,\mathrm{exp}}$ and the second stage by $k_{2,\mathrm{sqrt}}$, where it is also verified: $k_{2,\mathrm{exp}} < k_{2,\mathrm{sqrt}}$.

It is certainly important to mention that the initial silver consumption rate ν_{Ag} is approximately equal to the initial doped-layer built-up rate $\nu_{2,\mathrm{exp}}$ (obtained from the second composite function, i.e. the single exponential and the square root term). To explain almost perfect agreement found between the rates ν_{Ag} and $\nu_{2,\mathrm{exp}}$, we suggest an interpretation mainly based on the previous Rutherford backscattering spectroscopy (RBS) results (Wagner *et al.* 1997), which clearly showed a very high concentration of silver (around 80 at.% Ag) in the photodoped layer, at the beginning of the PD process.

3.2. *MDSC*

The results of the thermal analysis (MDSC) are summarized in table 1, which compares the glass transition temperature (T_g), the specific heat capacity (C_p) and the specific heat capacity difference (ΔC_p), for both layers and bulk glasses. The T_g

Table 1. MDSC results of the samples studied.

Glass sample	T_g from C_p (°C)	C_p (50°C) (J (g °C)$^{-1}$)	C_p ($0{\cdot}9T_g$) (J (g °C)$^{-1}$)	ΔC_p (J (g °C)$^{-1}$)
$As_{33}S_{67}$ bulk	157.57	0.4698	0.5185	0.2241
$As_{33}S_{67}$ film	159.62	0.3400	0.4211	0.2039
Ag/$As_{33}S_{67}$ photodoped film	152.80	0.2919	0.3510	0.2087
$AgAsS_2$ bulk	153.70	0.3335	0.3864	0.2247
Ag_3AsS_3 bulk	151.56	0.3015	0.3584	0.1619

value of the layer and bulk $As_{33}S_{67}$ glasses decreases slightly after silver (e.g. around 18 at.% Ag) is photodoped into the $As_{33}S_{67}$ layer or introduced in As–S bulk glass during the synthesis of the Ag–As–S glass in amounts of 25 and 43 at.% Ag.

The specific heat capacities C_p were measured by MDSC in heating scans in the glass transition temperature region. The C_p values reveal a significant decrease when silver is introduced into the $As_{33}S_{67}$ structure, and can be explained by the well known Debye model of heat capacities in solids (Wunderlich 1990), which relates the microscopic vibrations in solids to their heat capacities.

The specific heat capacity difference ΔC_p was also determined and this structure-sensitive parameter did not show a significant change for the $As_{33}S_{67}$ chalcogenide layer or bulk glass, after up to $\approx$ 25 at.% Ag is introduced. However, the change in structure is clearly more evident for the Ag_3AsS_3 bulk glass.

3.3. *Far-IR spectroscopy*

The structures of undoped, silver photodoped or silver 'melt-reacted' material were determined by FTIR absorption spectroscopy. The vibrational spectra of the light-exposed $As_{33}S_{67}$ layers, photodoped samples in PD stages 1 and 2, and crystals of Ag_3AsS_3 and Ag_2S are presented in figure 7. The FTIR transmission spectra of $AgAsS_2$ and Ag_3AsS_3 glasses are for a comparison taken from Jun *et al.* (1988), and are visualized as the inset of figure 7. There are strong absorption bands at 375 and 310 cm^{-1} in the spectrum of the undoped $As_{33}S_{67}$ film (figure 7, curve a). Significant IR bands appear in the spectra of the silver-doped samples (figure 7, curves b and c) at 380, 342, 310, 235 and 190 cm^{-1}, together with a weak vibrational band at 130 cm^{-1}. The distinct IR bands were obtained in spectra of crystalline Ag_3AsS_3 (proustite) at 337, 310, 263, 235 and 190 cm^{-1}, together with a weak absorption band at 130 cm^{-1}. The spectra of crystalline Ag_2S contains strong vibrational bands at 220, 184 and 130 cm^{-1}.

§4. Discussion

4.1. *The solid-state reaction and the diffusion model*

The solid-state chemical reaction and the proposed diffusion model is clearly supported by *all* the *analytic* techniques used in the present work. The kinetic data obtained are characterized by two rate coefficients, which implies that the PD phenomenon involves two different consecutive processes. It is suggested that in stage 1 (the exponential stage) a Ag-doped layer is formed. According to the previous results of RBS measurements already mentioned in this paper, the Ag-concentration profile of the photodoped $As_{33}S_{67}$ layer in the early stages of the PD process has, certainly, a quite complex character. The Ag-concentration profile is characterized initially by an

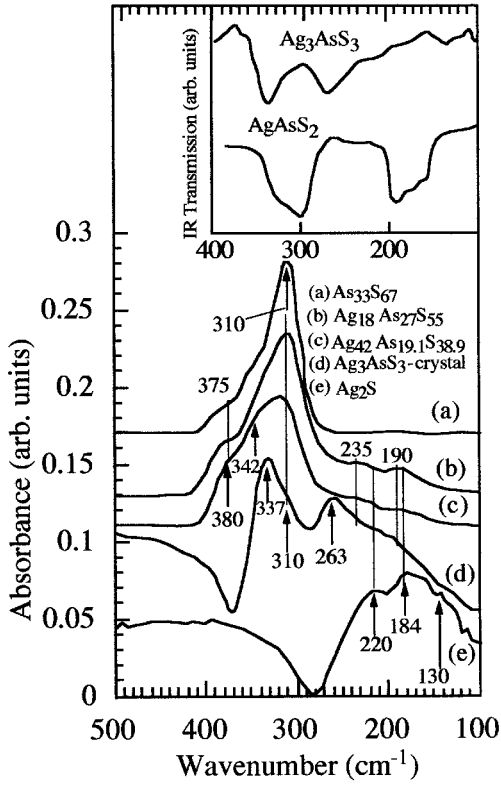

Figure 7. IR spectra of thin layers and bulk glasses in the As–S and Ag–As–S systems.

exponential dependence on the depth into the photodoped layer, but this dependence changes during the PD process into a step-like profile, as reported in Wagner *et al.* (1997), and previously for the Ag/As_2S_3 bilayer system (for example Yamamoto *et al.* (1976)). It is suggested that at the beginning of the first (exponential) stage of the PD effect, when the Ag-doped layer is formed and is *sufficiently* thin, the process can be influenced by space electric charges, resulting from the presence of a contact potential on the metal/p-type semiconductor boundary, which is the case for the $Ag/As_{33}S_{67}$ bilayer system, by illumination or heating of the chalcogenide layer. The light is absorbed near the free surface of the chalcogenide (i.e. at a depth $\ll 1\,\mu m$). Then, the electrons and holes are both excited. For triggering of the PD process, in the first stage of the two-stage model described by Arai *et al.* (1989), photons with energy either higher or lower than $E_{g,opt}$ are effective, and these photons influence the concentration of free carriers and, therefore, the rate of PD. The electrons may be trapped within a short distance, charging S atoms negatively. In contrast, the holes can traverse over 10 μm (Tanaka 1991), through the multiple-trapping processes. It is assumed that holes are able to enter directly (at the very beginning) into the Ag layer to induce the PD process. As the Ag-doped layer is built-in and separates the silver layer from the undoped chalcogenide layer, the holes can temporarily create sufficient electric fields across the Ag/Ag-doped/undoped boundaries, and the rate of PD is maintained, due to the tunnelling of electrons out of the metal, through the thin silver-doped layer up to the doped–undoped interface, as demonstrated in figure 8(*a*). As the thickness of the doped layer increases, the tunnelling process slows

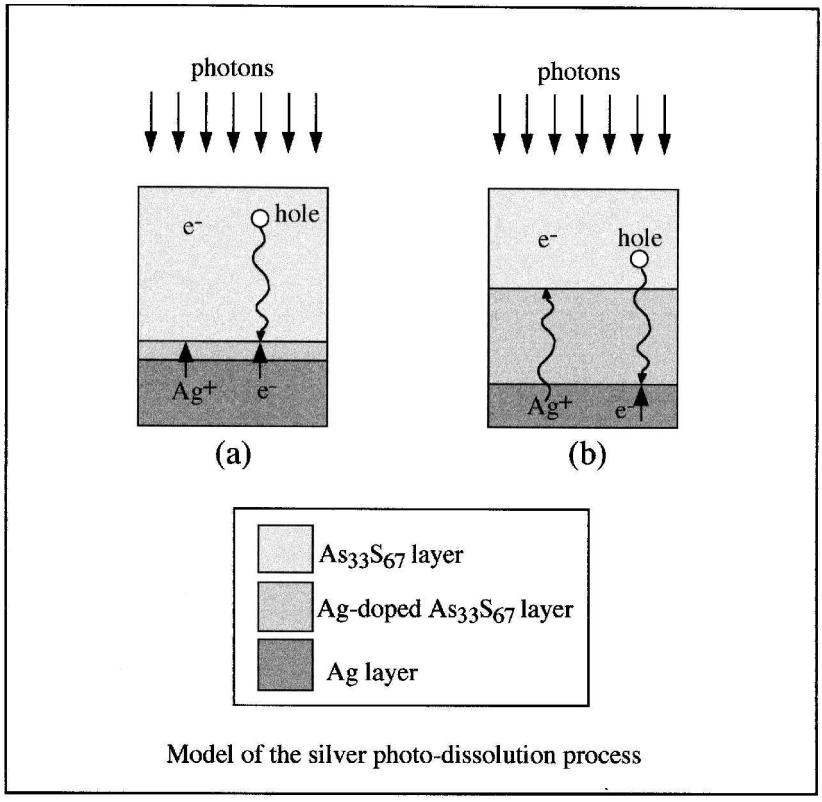

Figure 8. Schematic diagram of the proposed model for the PD process in the $Ag/As_{33}S_{67}$ system.

down remarkably. These types of processes are frequently found during the formation of thin surface oxide layers on metals at low temperatures and are described by an exponential or a logarithmic rate law (Schmalzried 1974).

Then, the holes have to diffuse through the silver-doped layer, towards the Ag/Ag–As–S boundary, in order for the PD process to progress further. Consequently the Ag^+ ions diffuse in the opposite direction towards the Ag–As–S/As–S boundary, where they react with undoped chalcogenides, as shown in figure 8(*b*). As the PD process continues and the thickness of the photodoped layer consequently increases, the *driving force* of the process becomes controlled by the solid-state chemical reaction on the $Ag/Ag–As–S/As_{33}S_{67}$ boundaries, where the slowest process obviously dictates the overall photoreaction rate. This slowest process is most probably located on the $Ag\text{-}As–S/As_{33}S_{67}$ boundary, where the reaction of Ag^+ ions with undoped chalcogenide takes place. It is important to note that the difference in chemical potential $\Delta\mu_{Ag}$ at the boundaries is also the key factor for these reactions. A measure of the chemical potential of silver is its corresponding isothermal activity a_{Ag}. This isothermal activity depends on the silver molar fraction in the Ag–As–S ternary system (Wagner *et al.* 1993), which has a finite range of homogeneity. It should be emphasized that the change in the chemical potential $\Delta\mu_{Ag}$ varies, depending on the silver content in the photodoped layer. At the beginning of the PD process the silver layer is the source of Ag atoms. The source of Ag ions is changed as the PD process

progresses. The Ag source becomes either a solid solution containing nearly 80 at.% Ag or a glass phase with a composition at the Ag-rich boundary of the glass-forming region, i.e. with a composition corresponding approximately to Ag_3AsS_3, as shown in Wagner *et al.* (1997). We should emphasize that the Ag-doped layer formation is controlled by the complex processes that take place in the exponential phase of the studied kinetic curve, i.e. stage 1.

The second stage of the PD process could be described either by a linear law (rate) or by a parabolic law (rate), as shown by the fitting procedure in figures 6(*b*) and (*c*). The linear law for a solid-state reaction is described in Schmalzried (1974), and refers to a process where its driving force is controlled by a solid-state chemical reaction. As the PD process continues, the Ag-doped region with a composition corresponding nearly to the stoichiometric compound $AgAsS_2$, could be formed, as reported by Wagner *et al.* (1997). As a result of this change, the difference of the chemical potential changes, which, consequently, gives a photo-induced reaction of a different rate, as discussed in relation with the two-stage exponential/linear model Wagner *et al.* (1997); the linear rate was also reported in Wagner *et al.* (1993) for $As_{33}S_{67}$ layer thicknesses of up to around 1 μm. The thickness of the $As_{33}S_{67}$ layer used in present work is 1·4 μm, and the mechanism of the PD reaction could be similar, as in the case of an $As_{33}S_{67}$ layer with thickness around 1 μm. It should be mentioned that in the present work, $k_{1,\mathrm{exp}} < k_{1,\mathrm{lin}}$, in comparison with the results reported by Wagner *et al.* (1993, 1997), where $k_{\mathrm{exp}} > k_{\mathrm{lin}}$.

In view of the better correlation suggested by the parameters R^2 and χ^2, in the fitting of the experimental data, the second stage of the reaction can more probably be described by a *parabolic* rate, as shown in figure 6(*c*), which is very common for solid-state chemical reactions, e.g. Schmalzried (1974) and Onari *et al.* (1985). The parabolic rate refers to a reaction where the driving force of the process is controlled mainly by diffusion. The average gradient of the chemical potential, which is responsible for the diffusional currents in the reaction product, is inversely proportional to the product-layer thickness Δx at any time. Furthermore, the instantaneous rate of increase in thickness $\mathrm{d}(\Delta x)/\mathrm{d}t$ is proportional to $1/\Delta x$. This relationship can be easily integrated to give the parabolic law for a photo-induced solid-state reaction, in the form: $(\Delta x)^2 = 2kt$. The reaction-rate constant, k, in this expression, is related to the parameter C_3 in the fitting function in figure 6(*c*). Almost perfect agreement between the initial silver-consumption rate ν_{Ag} and the initial doped-layer built-up rate $\nu_{2,\mathrm{exp}}(\nu_{\mathrm{Ag}} \approx \nu_{2,\mathrm{exp}})$, and the better correlation found in the parameters R^2 and χ^2, in the fitting of the experimental data, give strong support to the proposed two-stage exponential/square root model.

4.2. *Far-IR and MDSC*

Our results from far-IR spectroscopy and MDSC also prove clearly that the whole PD process is not just a simple diffusion, but rather a complex process involving a solid-state reaction, part of which, of course, entails diffusion. MDSC measurements, which have *not* been carried out on photodoped samples before, and IR spectra show that silver is chemically bonded to the host $As_{33}S_{67}$ amorphous matrix, but in different ways, at different stages of the PD process. We expect, therefore, the same composition of the reaction products as in Wagner *et al.* (1997), based on the results of RBS spectroscopy in the same $Ag/As_{33}S_{67}$ system.

All the structure-sensitive parameters, T_g, C_p and ΔC_p (see table 1), prove that a change occurs in the structure of $As_{33}S_{67}$ glass, as silver is introduced by photodop-

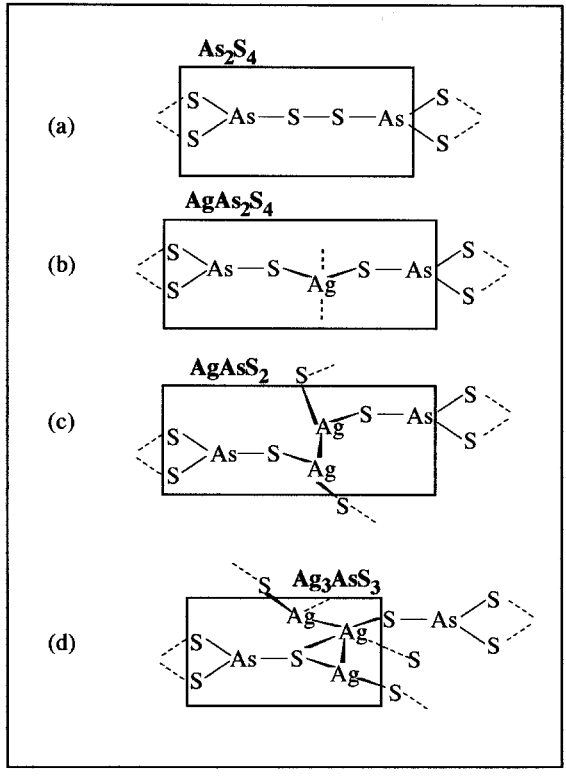

Figure 9. The structure of the $As_{33}S_{67}$ and Ag–As–S glasses. Structures (*a*) and (*b*), (*c*), (*d*) are for undoped and Ag photodoped films, respectively, during the course of the PD process.

ing or melt-quenching. This is also clear from the IR spectra in figure 7. The structure of $As_{33}S_{67}$ layers is based on a network of the AsS_3 structural units (Onari *et al.* 1985), as shown in figure 9(*a*), which have characteristic IR bands at 310, 342 and 375 cm^{-1}. These bands are present in the IR spectra after the introduction of Ag (see figure 7, curves b and c) into the amorphous $As_{33}S_{67}$ matrix. The presence of Ag in the glass structure results in a continuous spectrum also containing new features, i.e. vibrational bands at 235 and 190 cm^{-1} and a very weak band at 130 cm^{-1}, which are characteristic of $AgAsS_2$, Ag_3AsS_3 and Ag_2S compounds, and are described in Jun *et al.* (1988) as Ag–S stretching and S–Ag–S bending vibrations. These IR bands are presented in figure 7, curves d and e, and in the inset, the IR transmission spectra from Jun *et al.* (1988).

The structure of the Ag-doped glasses is based on single or multiple AsS_3 pyramidal units, linked via Ag atoms. The expected structural changes with increasing silver concentration in the $As_{33}S_{67}$ structure, derived from the X-ray diffraction structural studies by Gould (1993), of their crystalline counterparts, is shown in simplified form in figures 9(*a*)–(*d*).

§5. Conclusions

In the present paper, we have been able to carefully monitor the kinetics of the PD process in thicker $As_{33}S_{67}$ glass films ($d = 1{\cdot}4\,\mu m$). The kinetics of the reaction

was described by two consecutive processes with different rate coefficients. The first and second reaction stages were attributed to exponential and linear or to exponential and parabolic rate laws, respectively. It was clearly shown that the second kinetic stage cannot be related to the elemental silver-source exhaustion.

The structure of the reaction product has been studied by the novel technique, Modulated Differential Scanning Calorimetry and also by far-FTIR spectroscopy. A comparison of the glass transition temperature T_g, the specific heat capacities C_p and the specific heat capacity difference ΔC_p for the photodoped layers and the Ag-containing bulk glasses, has been carried out. The T_g and C_p values of the layer and bulk $As_{33}S_{67}$ glasses decrease slightly after the Ag (e.g. 18 at.%) is photodoped into the $As_{33}S_{67}$ layers, or when the Ag (25 and 43 at.%) is introduced in the $As_{33}S_{67}$ bulk glass during its synthesis. The far-FTIR spectra show that there are strong absorption bands at 375 and 310 cm^{-1} for the undoped $As_{33}S_{67}$ glass film. Significant IR bands appear in the spectra of the silver-doped samples at 380, 342, 310, 235 and 190 cm^{-1}, together with a weak vibrational band at 130 cm^{-1}.

Acknowledgments

The authors are grateful to Dr V. Smrčka, (Joint Laboratory of Solid State Chemistry of the Academy of Sciences and of the University of Pardubice, 530 09 Pardubice, CR) for FTIR measurements. One of the authors (T.W.) is grateful for financial support from the European Community under Grant ERBCIPA CT940107, Grants 203/96/0876 and 203/98/0103 Grant Agency of Czech Republic.

References

Arai, T., Wakayama, Y., Kudo, H., Kishimoto, T., Lee, J., Ogawa, T., and Onari, S., 1989, *J. non-crystalline Solids,* **114**, 40.

Ewen, P. J. S. , Zakery, A., Firth, A. P., and Owen, A. E., 1988, *Phil. Mag.* B, **57**, 1.

Fernandez-Pena, J., Ramirez-Malo, J. B., Ruiz-Perez, J. J., Corrales, C., Marquez, E., Villares, P., and Jimenez-Garay, R., 1996, *J. non-crystalline Solids,* **196**, 173.

Firth, A. P., Ewen, P. J. S., and Owen, A. E., 1985, *J non-crystalline Solids,* **77&78**, 1153.

Goldschmidt, D., and Rudman, P. S., 1976, *J. non-crystalline Solids,* **22**, 229.

Gould, R. O., 1993, private communication. Crystal structure data available from Inorganic Crystal Structure Data, Institute of Inorganic Chemistry, University of Bonn, and the Gmelin Institute, were used in the CALC Program for Molecular Geometry, by R. O. Gould and D. Taylor, University of Edinburgh, 1993.

Jun, L., Videau, J. J., Tanguy, B., Portier, J., Reau, J. M., and Hagenmuller, P., 1988, *Mater. Res. Bull.,* **23**, 1315.

Kolobov, A. V., and Elliot, S. R., 1991, *Adv. Phys.,* **40**, 625.

Kosa, T. I., Wagner, T., Ewen, P. J. S., and Owen, A. E., 1995, *Phil. Mag.* B, **71**, 311.

Kostyshin M. T., Mikhailovskaya, E. V., and Romanenko, P. F., 1966, *Sov. Phys. Solid State,* **8**, 451.

Marquez, E., Fernandez-Pena, J., Gonzalez-Leal, J. M., and Jimenez-Garay, R., 1995, *Mater. Lett.,* **25**, 143.

Marquez, E., Jimenez-Garay, R., Zakery, A., Ewen, P. J. S., Owen, A. E., 1991, *Phil. Mag.* B, **63**, 1169.

Onari, S., Asai, K., and Arai, T., 1985, *J non-crystalline Solids,* **76**, 243.

Reading, M., 1993, *Trends Polym.,* **1**, 248.

Reading, M., Elliott, D., and Hill, V. L., 1993, *J. Thermal Anal.,* **40**, 949.

Reading, M., Luget, A., and Wilson, R., 1994, *Thermochim. Acta,* **238**, 295.

Sauerbrunn S., Crowe, B., and Reading, M., 1992, *Am. Lab.,* August, 44.

Sauerbrunn, S., and Thomas, L., 1995, *Am. Lab.,* January, 19.

Schmalzried, H., 1974, *Solid State Reactions* (New York: Academic Press), pp. 145–172.

Tanaka, K., 1991, *J. non-crystalline Solids,* **137&138**, 1021.

WAGNER, T., FRUMAR, M., and BENES, L., 1987, *J. non-crystalline Solids,* **90**, 517.
WAGNER, T., and KASAP, S. O., 1996, *Phil. Mag.* B, **74**, 667.
WAGNER, T., PERINA, V., VLCEK, M., FRUMAR, M., RAUHALA, E., SAARILAHTI, J., EWEN, P. J. S., 1997, *J. non-crystalline Solids,* **212**, 157.
WAGNER T., VLCEK, M., NEJEZCHLEB, K., FRUMAR, M., ZIMA, V., PERINA, V., and EWEN, P. J. S., 1996, *J. non-crystalline Solids,* **198&200**, 744.
WAGNER, T., VLCEK, M., SMRCKA, V., EWEN, P. J. S., and OWEN, A. E., 1993, *J. non-crystalline Solids,* **164&166**, 1255.
WUNDERLICH, B., 1990, *Thermal Analysis* (New York: Academic Press), pp. 253–276.
WUNDERLICH, B., JIN, Y., and BOLLER, A., 1994, *Thermochim. Acta,* **238**, 277.
YAMAMOTO, Y., ITOH, T., HIROSE, Y., and HIROSE, H., 1976, *J. Appl. Phys.,* **47**, 3603.